d-Au Multiplicity Analysis Note
S.J. Sanders

Contents

Overview.

The analysis of the charged particle pseudorapidity densities for the d-Au run at $\sqrt{s_{NN}}$ =200 GeV follows closely that used for the Au-Au analyses at $\sqrt{s_{NN}}$ =130 GeV [1] and 200 GeV[2]. These earlier analyses are described in some detail in an earlier Brahms Analysis Note[3] and in the Ph.D. dissertation of H. Ito.[4] Although the d-Au analysis is similar to that done earlier for the heavier system, the significantly lower charged particle multiplicities found for the d-Au measurement leads to some systematic errors becoming significant that could earlier be neglected. Also, the reconfiguration of the Si Multiplicity Array (SiMA) electronics to remove the PTQ's also leads to changes in the analysis procedures. This Note describes in detail the d-Au analysis.

The general steps for converting analog outputs from the SiMA and the Tile Multiplicity Array (TMA) to a deduced charged-particle density are summarized below. The remainder of the note expands on these steps and presents the final results.

Steps followed for the multiplicity analysis are:

A. The analog signals are digitized. As stated above, there was a change in the d-Au run for the SiMA where we removed a x10 attenuation of the signal before digitization using an 11-bit FERA. The TMA digitization was unchanged from the earlier Au-Au run.
B. The ADC signals are energy calibrated using the single-MIP response in the detector. This step was unchanged.

C. The measured energy in each detector element is converted to the corresponding number of charged particles hitting that element, N_{ch}, using a conversion function that depends on the distance of the collision vertex from the detector element. This conversion function can be expressed in terms of the pseudorapidity of the particle η. Because the secondary scattering background depends on the overall $dN_{ch}/d\eta$ distribution, new conversion functions were generated for the d+Au run based on Geant simulations. The conversion function developed for the SiMA d+Au data also introduces an implicit "correction" for saturation events: these events are suppressed both in developing the conversion function and in the use of this function.

D. The geometry of the detector element (width, height, distance from interaction vertex) is used to calculate $dN_{ch}/d\eta$ based on the previously determined value of N_{ch}. It should be noted that we only obtain a useful $dN_{ch}/d\eta$ determination after we take the average over a large number of events. For any given event, this value is strongly influenced by the Landau tail of the detector energy response.

E. Separate array multiplicities M are found for the SiMA and TMA. Since the array multiplicities depend on the location of the interaction vertex, the measured values are adjusted by a correction function to determine the equivalent multiplicity for a collision occurring at the geometric center of the Multiplicity Array (MA). This function should be deduced empirically based on the experimental data. The current function was found using GEANT simulations.

F. A weighted average is taken of the SiMA and TMA array multiplicities. The weighing is a fixed number that adjusts the SiMA results for the different effective coverage of the two arrays at the nominal vertex. This involves more than just the difference in solid angle of the SiMA and TMA as the overall $dN_{ch}/d\eta$ distribution also affects the scaling.

G. The weighed average determined in the previous step is converted to a centrality. Here it is assumed that, for example, the 10% of events with the highest value of M correspond to the 10% most central events. The multiplicity-to-centrality conversion function is determined using minimum biased experimental events and includes a correction for the inefficiency of our min-bias trigger.

Analysis Details.

Step A. Digitization

For the d-Au measurements (and also the pp measurements in run II) we removed the Peak-to-Charge (PTQ) modules from the signal path. Their removal results in a linear calibration between the energy loss in the detector and the channel to which this signal maps in the FERA. The PTQ's were found in the Au-Au measurements to have a very non-linear, compressed response for low amplitude input signals between the pedestal and an equivalent energy of about 100 keV (i.e., the single MIP energy for normal incident particles). We accounted for this non-linear response by applying a pulser derived correction.

Although an *in situ* verification of the SiMA calibration was not performed during the d+Au measurements (this should still be done!), earlier bench top tests of the preamp+shaper boards showed a very linear response to within the precision of the testing method (a few percent).

The PTQ units were also used to apply x10 attenuation to the input signal. This was essential for the Au+Au run to avoid excessive saturation of the 11-bit FERA. The lower particle densities for the d-Au measurement are offset by the loss of the x10 attenuation. Figure 1 compares the raw FERA signals for the si1_1 detector for the 200 GeV Au-Au run (with PTQ) and the 200 GeV d-Au run (without PTQ).

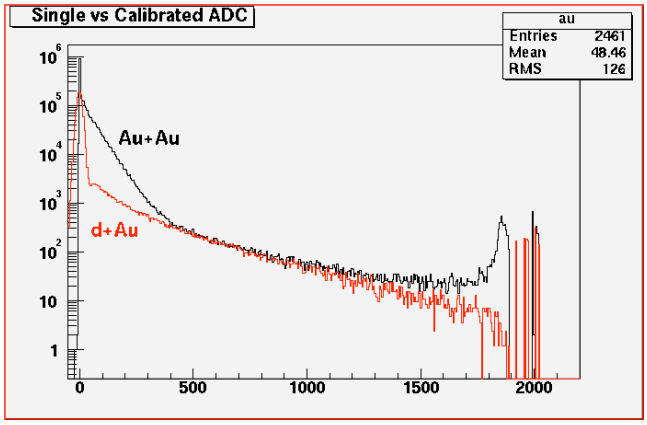

Fig. 1. Comparison of FERA spectrum for si1_1 (strips a-g summed) for the Au+Au run with the PTQ and the d+Au run without the PTQ. The d+Au data has been scaled to have approximately the same number of pedestal counts as for the Au+Au data.

Step B. Energy calibration

The energy calibration procedure was not changed for the d-Au run. For each Si (and Tile) detector element, geometry scaled ADC spectra are generated as a function of the displacement of the vertex from the detector element. The energy deposited in the detector increases with increasing displacement of the vertex because of the more oblique angle of incidence of the primary particles onto the detector. The geometry scaling amounts to multiplying the observed pedestal-subtracted ADC signal by sin(□), where □ is the angle of incidence of particles emitted from the vertex position. The resulting spectra show a peak corresponding to single-MIP particles. The location of this peak (in scaled ADC channels) is determined by fitting the spectrum with a Gaussian line shape superimposed on a linear background. The corresponding energy for the peak is determined from GEANT simulations of the detector response. Although the geometric sin(□) term accounts almost fully for the vertex dependence, there is a small residual effect resulting from the varying background contribution as the vertex moves further away from the detector. This residual correction as deduced with the GEANT simulations is shown in Fig. 2 for the Si and Tile arrays. The slope of the E vs. (calibrated ADC) is determined as the best fit value to reproduce the GEANT simulations. The residual, vertex-dependent correction for the single-MIP energy resulting from the background could be different for the d-Au and Au-Au runs. Because this is a small effect, however, a new correction function has not yet been developed for the d-Au run.

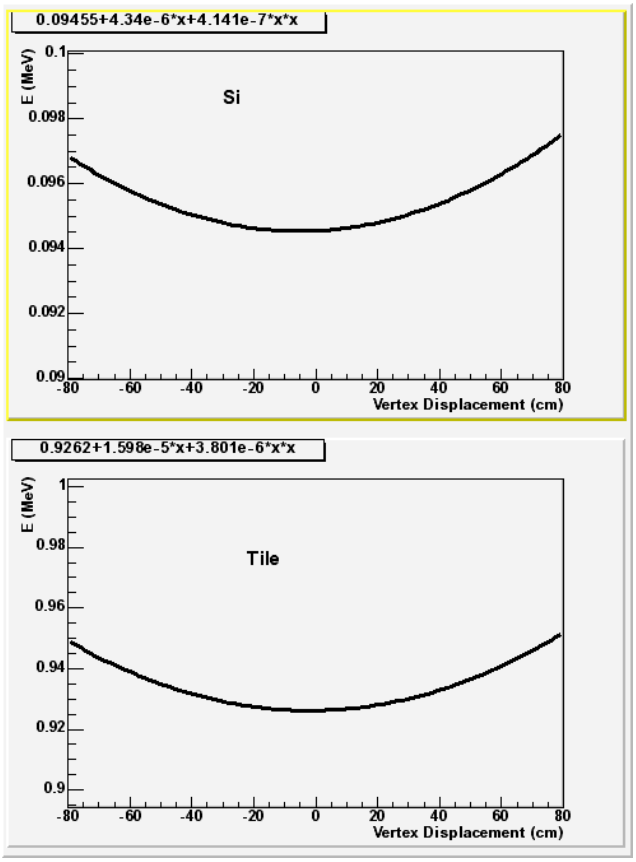

Fig. 2—Geometry corrected energy of single-MIP peak as a function of the displacement of the vertex from the detector element.

Figures 3 and 4 show comparisons of the energy calibrated spectra observed in the si1_1 and si1_4 wafers for the d-Au data run compared to the corresponding GEANT simulated spectrum.

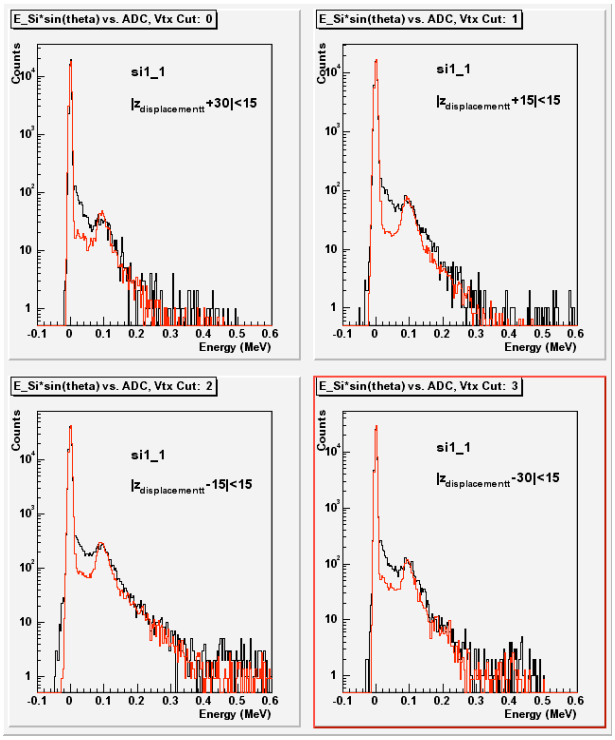

Fig. 3–Comparison of Geant simulation to d+Au data for the si1_1 wafer. The vertex displacement is as indicated. The simulated spectrum has been scaled to have the same number of counts in the pedestal as found for the data. The si1_1 wafer is an example of a "typical" resolution detector.

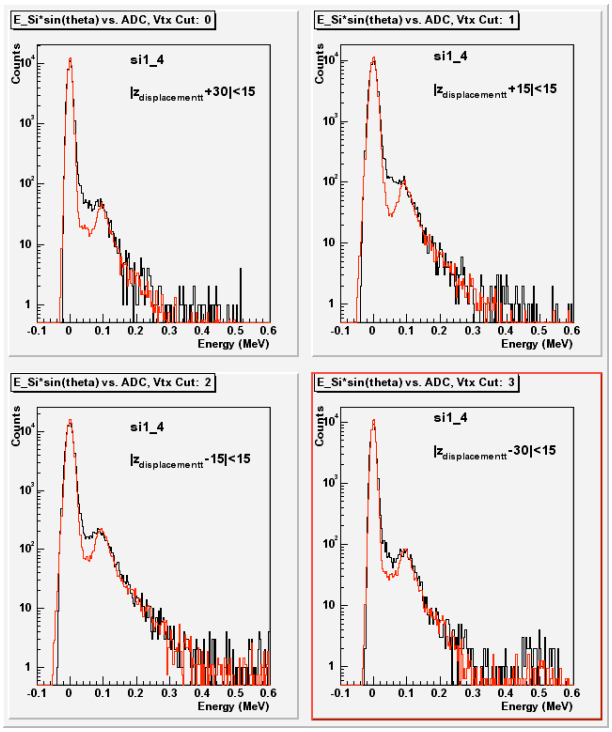

Fig. 4–Comparison of Geant simulation to d+Au data for the si1_4 wafer. The vertex displacement is as indicated. The simulated spectrum has been scaled to have the same number of counts in the pedestal as found for the data. The si1_4 wafer is typical of the "poor" resolution detectors.

Step C. E to N_{ch}

The conversion function is calculated by taking a large number of simulated central-collision events for vertex positions ranging from a nominal position between –80 cm and +80 cm from the geometric center of the MA. The N_{ch} (primary) and corresponding "detected" energy E for each detector element are summed into two separate histogram arrays as a function of □. After analyzing a large number of events, the N_{ch} array is divided by the detected energy array to obtain the conversion function. This procedure does NOT give the same result as would be obtained by taking an average of N_{ch}/E calculated event-by-event. The Landau shape of the deposited energy distribution prevents us from using this latter procedure.

In determining the energy calibration, simulated events with energy below the assumed threshold (typically 3 to 5 times the pedestal width) were set to have zero energy. Events corresponding to ADC saturation were suppressed. A vertex position resolution of 2.5 cm was assumed in calculating □-values used for sorting the events. Figure 5 and 6 show the

resulting N_{ch}/E vs. □ functions for the SiMA and TMA, respectively. As done for the Au+Au data, a single function is used the SiMA and eight separate functions are used for the TMA, corresponding to each of the eight rings. In Fig. 5 the thick black line shows the adopted function, while the colored curves show the individual functions for each of the six Si wafer locations along the beam line.

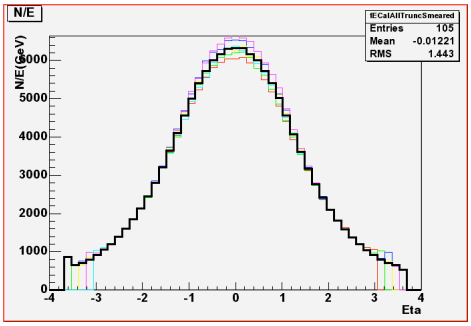

Fig. 5–N_{ch}/E vs. □ for SiMA. The solid black line is the calibration adopted for the analysis. The different color curves show the corresponding calibrations for each of the six Si rings.

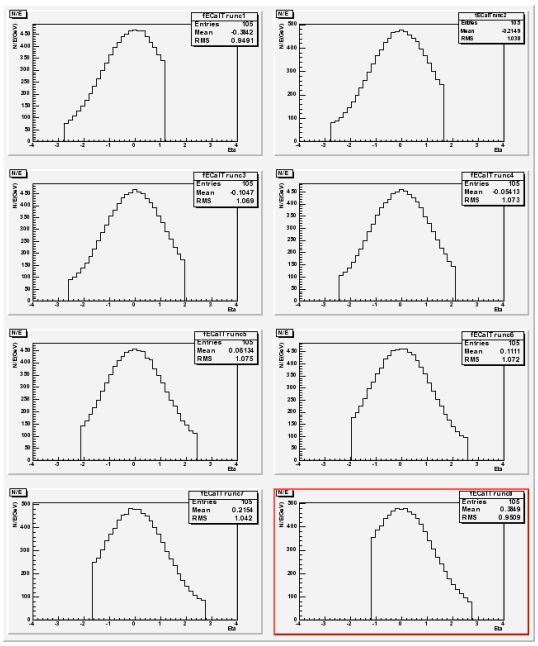

Fig. 6– N_{ch}/E vs. □ for TMA. Separate calibrations are used corresponding to each of the tile rings.

A calibration was also done where the saturation events were used in the calibration, setting the corresponding energy to the saturation energy, but this was found to result in a calibration where a replay of the simulated data failed to reproduce the Hijing input distribution. Fig. 7 compares the SiMA calibration obtained by suppressing the saturation events with the calibration found by assuming these events convert to the saturation value for the ADC (i.e., channel 2047). This figure also shows the effect of the vertex position resolution. This resolution is taken as 2.5 cm, consistent with the observed vertex resolution based on the BB counters.

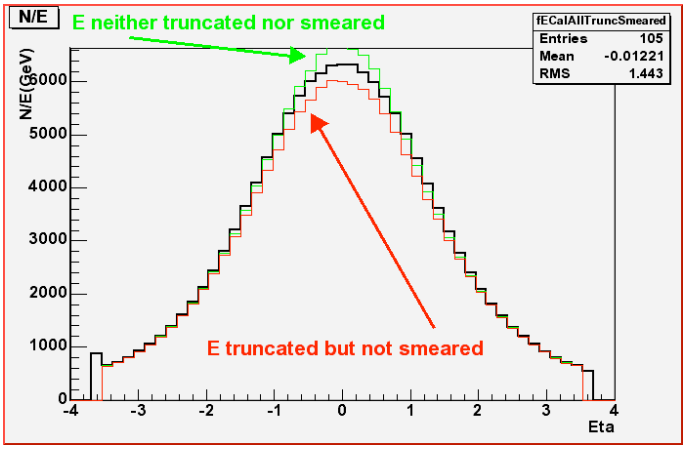

Fig. 7–Comparison of N_{ch}/E calibrations obtained with different treatments of saturated events (suppressed or not suppressed) and the experimental vertex resolution (the "smearing" assumes a 2.5 cm resolution.)

Step D. Calculation of $dN_{ch}/d\eta$

Although a value for $dN_{ch}/d\eta$ is calculated for each detector element and for each event, it is only when these values are averaged over many events that one can expect reasonable results. This is a consequence of the Landau form of the energy loss distribution with its extended high-energy tail. For the analysis of the SiMA, two 2-D histograms were created: 1) for each event and detector element, the corresponding $dN_{ch}/d\eta$ value was summed into a centrality vs. η histogram, 2) the number of $dN_{ch}/d\eta$ entries were stored in a second centrality vs. η histogram with the same bin resolution. Dividing these two histograms gives the $<dN_{ch}/d\eta>$ value for each value of centrality and η. The same procedure was followed for the TMA.

Step E. Correction of array multiplicity for vertex location

The measured charged-particle multiplicity in the SiMA and TMA will depend on the vertex location since the effective solid angle and pseudorapidity coverage depend on this location. For the BRAHMS analysis we correct for this dependence by developing vertex dependent scaling functions for the SiMA and TMA that take the multiplicities measured at some distance from the nominal vertex and converts this to the equivalent multiplicity for the nominal vertex.

Figure 8 shows the mean multiplicity (using the ROOT Profile method) as a function of vertex position for the SiMA and TMA based on a GEANT simulation using 0-2 fm Hijing events. The inverse of these fuctions, normalized to 1 at z=0, are used as a first approximation to correct the array multiplicity. Figure 9 shows the same GEANT simulation, but this time with the vertex correction applied to the multiplicity.

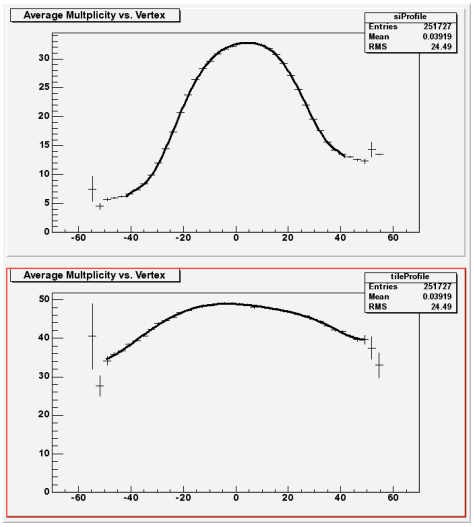

Fig. 8–Mean multiplicities for the SiMA and TMA as functions of vertex location. The solid lines are 9th order polynomial fits. The inverse functions, normalized to 1 at z=0, are used to correct the array multiplicity for vertex position. (For the SiMA a second iteration was need to achieve the results in Fig. 9.)

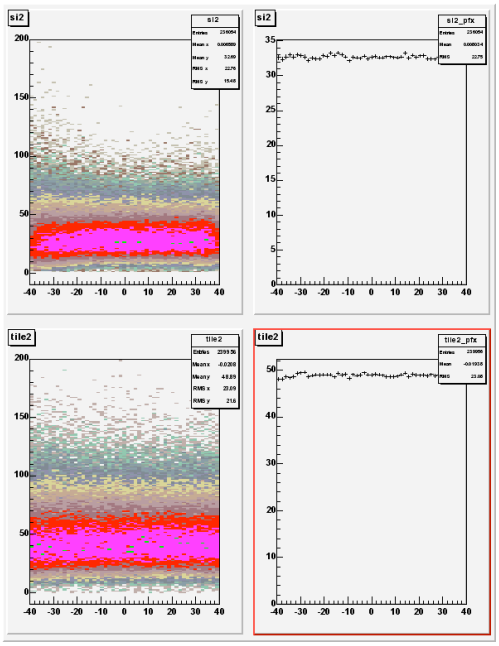

Fig. 9–Right: Corrected multiplicity distributions for SiMA(top) and TMA(bottom) as a function of the vertex location. Left: Corresponding mean multiplicities (Profile spectra).

The concern with this multiplicity correction is that it relies on the experimental distribution having the same behavior as the simulated data. The vertex correction function will be incorrect, for example, if the simulated pseudorapidity dependence if different from the experimental distribution. Fig. 10 shows the corrected SiMA and TMA multiplicity distributions based on experimental runs 8404 and 8405, selecting the min-bias trigger 5. One has to be careful in interpreting this figure since the color map is dominated by the vertex distribution of the collisions.

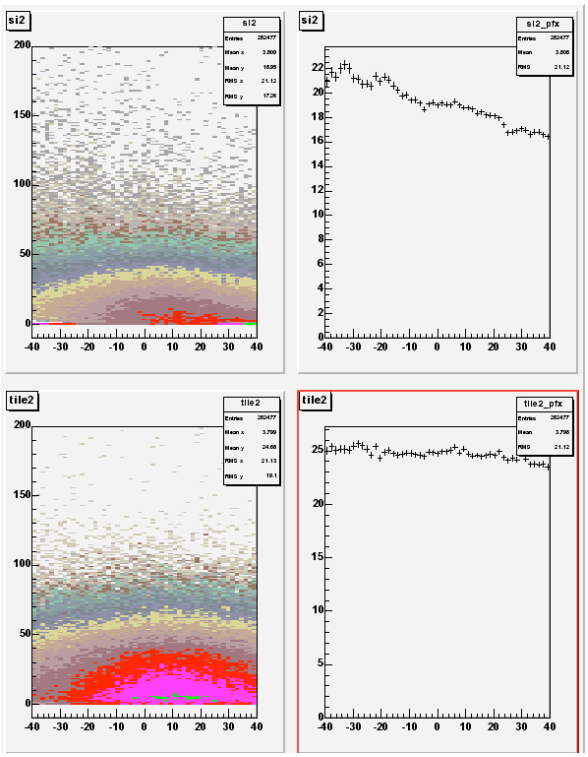

Fig. 10 – Same as Fig. 9, but with min-biased dAu data of runs 8404 and 8405.

Noticing that the TMA multiplicity has a much smaller vertex dependence, Fig. 11 shows the correlation of SiMA and TMA multiplicities for three different vertex cuts centered at –30 cm, 0 cm, and 30 cm, respectively, accepting data within +/- 10 cm of these values. The SiMA multiplicities have been scaled by a factor of 1.38, as discussed in the next section (Step F).

It appears from Fig. 11 that the correction used between 0 and –30cm is quite good, while there appears to be more of a problem going to +30cm. This is a different conclusion than one might take from inspection of Fig. 10. We should investigate this vertex dependence more carefully, possibly by selecting more central event based on the BB and/or ZDC array data.

The broader correlation functions found in moving away from z=0 cm and particularly noticeable for z=-30cm may reflect lower hit densities associated with the $dN_{ch}/d\eta$

distribution. Vertices at z=-30cm are outside of the SiMA and, consequently, will correspond in all cases to positive values of , where the particle densities are lower.

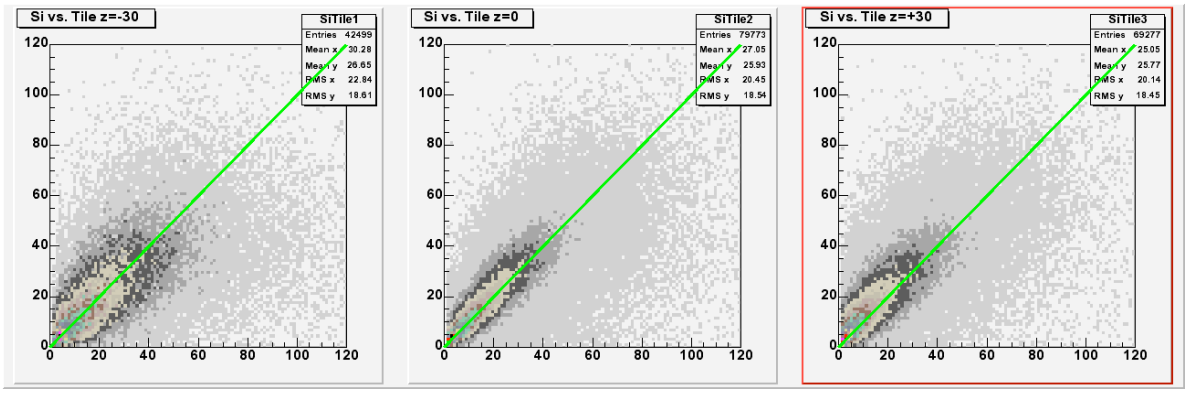

Fig. 11–SiMA multiplicity vs. TMA multiplicity vertex locations (left-to-right) of –30cm, 0 cm, and 30 cm. The green lines show the loci of SiMA = TMA.

Step F. Find weighted average of SiMA and TMA multiplicities

The SiMA and TMA cover different solid angles and so to obtain an average multiplicity the SiMA result is scaled by an empirical factor. Although this factor is expected to be related to the different solid angle coverage of the two arrays, it is also influenced by the pseudorapidity dependence of the particle emission. For the 200 GeV Au+Au run, the average multiplicity was taken as $M = (M_{TMA}+1.66\ M_{SiMA})/2$. This changes for the d+Au run, with $M = (M_{TMA}+1.38\ M_{SiMA})/2$. Figure 11 shows plots of $1.38\ M_{SiMA}$ vs. M_{TMA} for different vertex locations. It is clear from these histograms that there is considerable scatter in the multiplicity values for the two array.

The value of the scaling function for the SiMA was obtained by determining the factor fSi that results in $\langle(fSi * M_{SiMA} - M_{TMA})/(M_{SiMA}+M_{TMA}+5.)\rangle = 0$. A plot of the function on the RHS is shown in Fig. 12, taking fSi = 1.38.

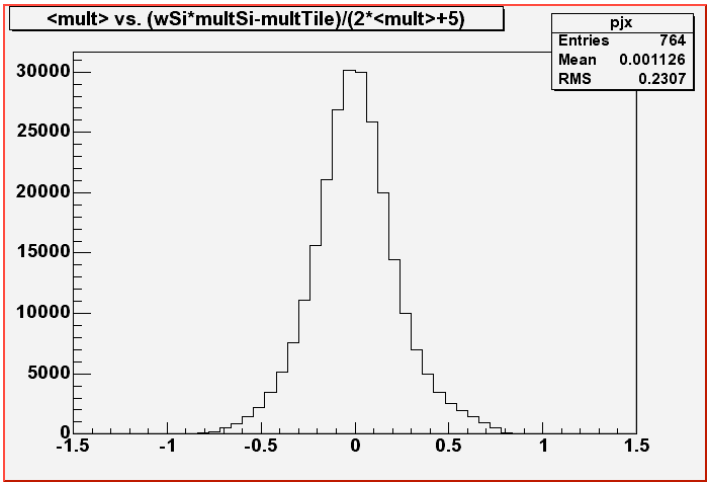

Fig. 12–Distribution used to establish SiMA scaling factor.

Step G. Centrality determination

It is assumed that there is a direct dependence of reaction centrality on charged particle multiplicity with, for example, the events with the 10% highest multiplicities corresponding to the 10% most central event. The complication with the d-Au data is that the lower particle densities result in this mapping being less well defined. This is evident in the comparison of the SiMA and TMA multiplicities in Fig. 11.

Figure 13 shows the individual multiplicity distributions for the SiMA and TMA as well as the average of these two multiplicities. As done for the Au-Au analysis, we again use the average multiplicity to determine reaction centrality.

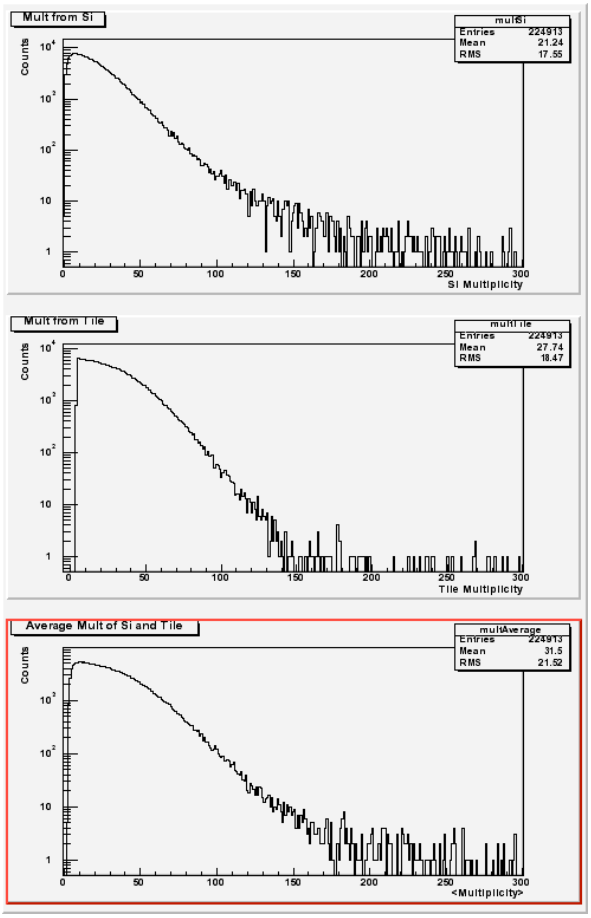

Fig. 13–Multiplicity distributions for the SiMA and TMA. The bottom panel shows the average of the SiMA and TMA distributions, with the SiMA distribution scaled by a factor of 1.38.

The calibration from multiplicity to centrality is done by first generating a histogram of centrality vs. multiplicity. From GEANT simulations it was determined that with the INEL trigger (our min-biased trigger) we should have an efficiency of 82.1% for detecting events with $M_{TMA}>4$ (assuming the nominal vertex location). The total event yield is then taken as

$Y_{tot} = \sum_{5} M_{TMA}$ /0.821. For a given value of the averaged multiplicity <M>, the corresponding centrality is then taken as: $C = 100 * \sum_{<M>} \left(M_{SiMA} + M_{TMA} \right) / 2 \sum Y_{tot}$. The curve of C vs. <M> is fitted in three ranges, as shown in Fig. 14.

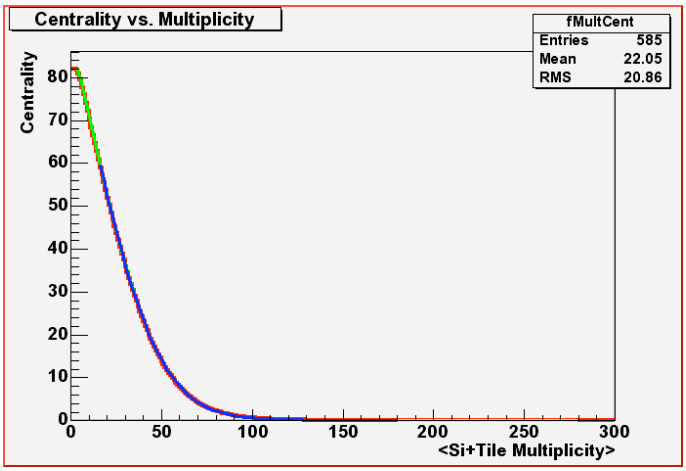

Fig. 14–Centrality vs. average of SiMA and TMA multiplicities. The red curve (hidden by the fits) shows the data. The green, blue and yellow curves are the fitted functions used to determine the centrality for a given value of <M>

The distribution of events as a function of centrality should be flat using this procedure. Figure 15 shows the distribution for data from run 8404.

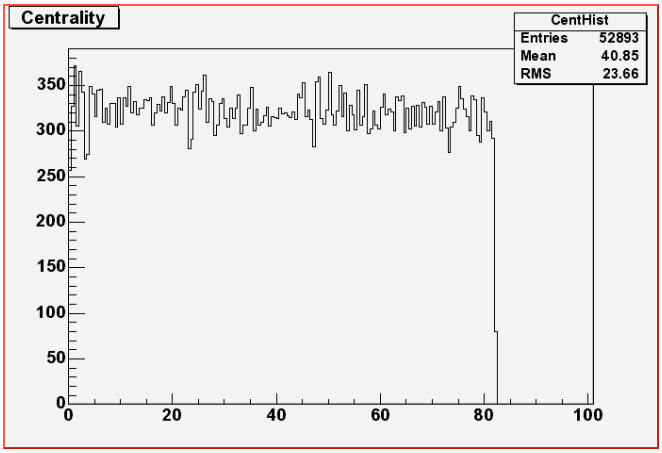

Fig. 15–Distribution of events as a function of reaction centrality.

$dN_{ch}/d\eta$ distributions

The charge-particle pseudorapidity density distributions for the SiMA and TMA are shown in Fig. 16 and 17. The figure show two centrality ranges: 0-30% and 30-60%, and are obtained with different assumptions of the SiMA energy threshold. The discrepancy between the SiMA and TMA results near η=0 is believed to result from our inability to correctly model

the SiMA energy spectra at low energy, as evident in Figs. 3 and 4. Varying the assumption as to how much of the yield between the pedestal and the single-MIP peak should be associated with "no-hits" events can strongly affect the SiMA distribution. For Fig. 16, the SiMA and TMA energy thresholds are taken as 3.5 and 3.0 times the width of the pedestal peak, respectively. The thresholds are increased to 4.0 times the respective pedestal width in Figure 17.

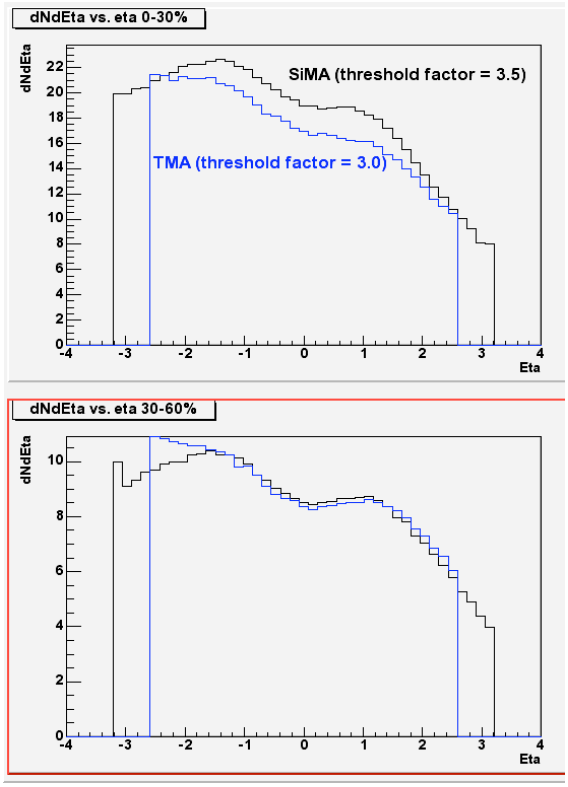

Fig. 16–$dN_{ch}/d\eta$ distributions for the SiMA (black) and TMA (blue) arrays. The centrality cuts are indicated in the figure.

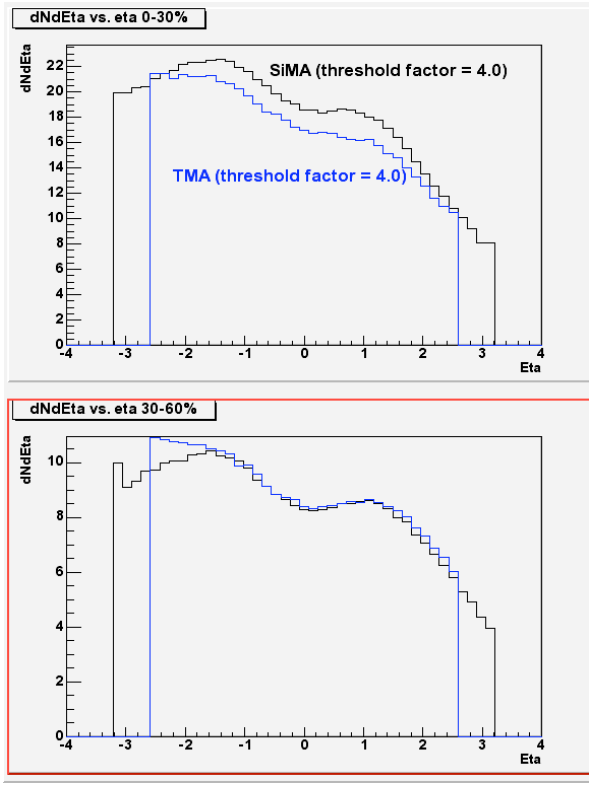

Fig. 17–Same as Fig. 16, but with energy threshold factor increased for the SiMA, as indicated.

The thresholds used for the analysis shown in Fig. 17 are illustrated in Fig. 18. The figure shows energy spectra at three different pseudorapidity values for the SiMA (left side) and TMA (right side). From this figure one sees that it will be hard to justify increasing the SiMA threshold any further without a realistic simulation of the low-energy detector response. The TMA threshold should be raised some more, although this is not likely to significantly change the results since the single-MIP energy is well removed from the pedestal.

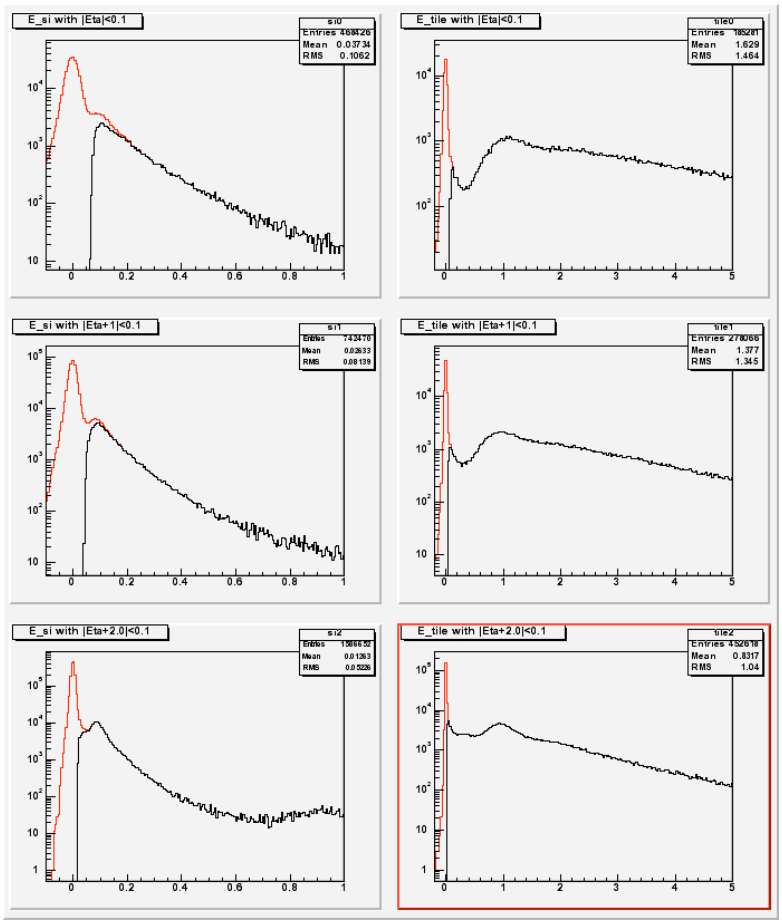

Fig. 18–Threshold used in analysis. The red curves indicate the regions of the energy spectra assumed to be below threshold and corresponding to "no-hit" events. The threshold are show for □=0,1, and 2 (top-to-bottom) for the SiMA (left) and TMA(right). The energy scales (abscissa) are in MeV.

HIJING

Figure 19 shows the $dN_{ch}/d\square$ distributions obtained with the GEANT simulations using the HIJING event generator for the primary event input. The red and green lines show the "actual" HIJING distributions for the SiMA and TMA, respectively. After passing these distributions through the analysis code one obtains the black (SiMA) and blue (TMA) spectra. Much of the discrepancy, most noticeable for the 30-60% centrality cut, can be attributed to the choice of energy threshold. Figure 20 shown the threshold behavior for the GEANT simulations.

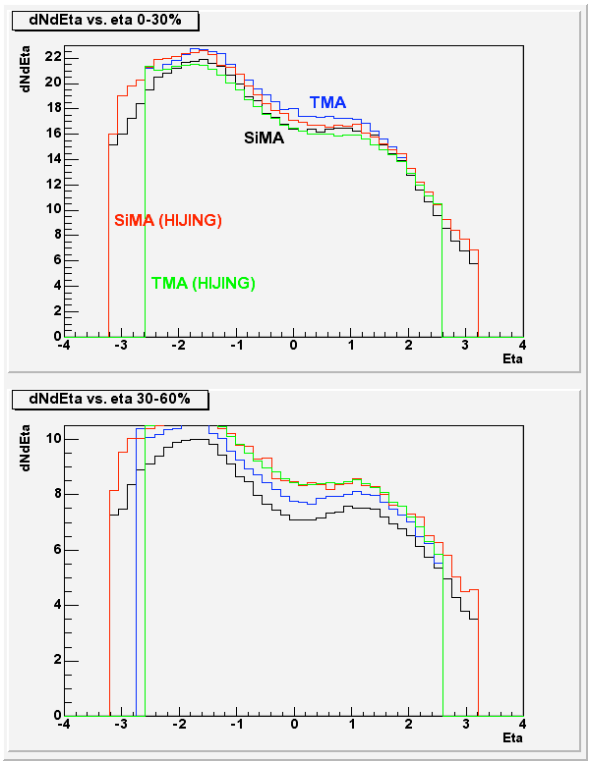

Fig. 19–GEANT simulations. The HIJING distributions used as input to the GEANT simulations are shown by the red and green curves. After running these through the analysis procedure, using a threshold factor of 4.0 for both arrays, the resulting "measured" distributions are shown by the black and blue curve.

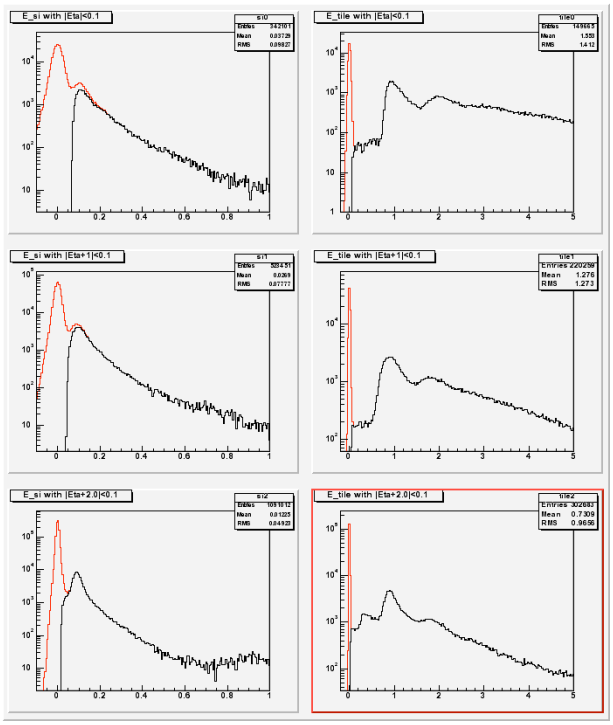

Fig. 20–Energy thresholds corresponding to GEANT analysis shown in Fig. 19.

Figure 21 compares the measured $dN_{ch}/d\eta$ distributions (0-30% central and 30-60% central) for the TMA with the corresponding HIJING input distributions. Although the extremely good agreement may be somewhat misleading since the comparison should be with the GEANT deduced spectra, it is still clear that the agreement is very good.

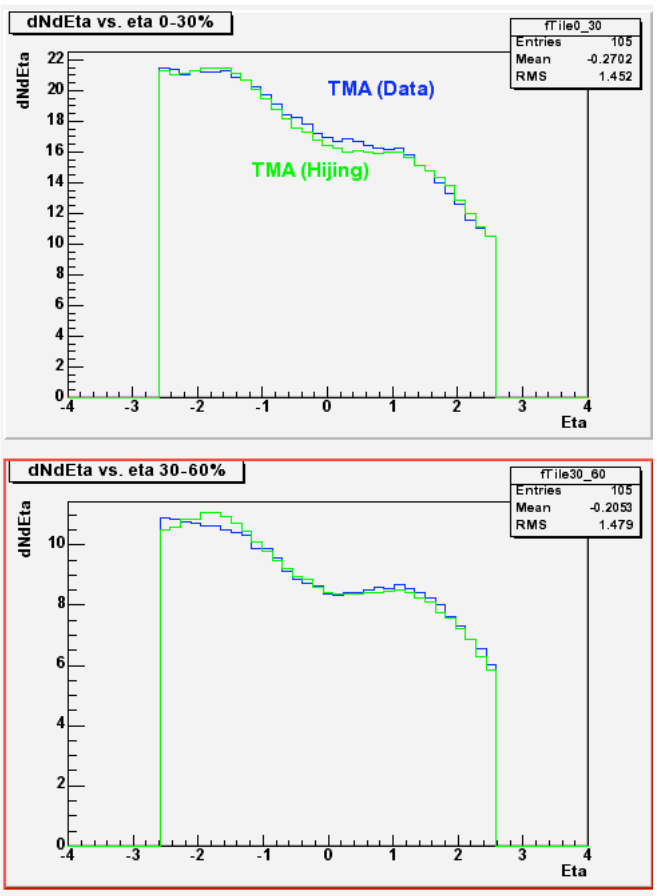

Fig. 21–Comparison of d-Au experimental results for the TMA with the corresponding HIJING distributions.

Conclusions

The d-Au data look remarkably like the HIJING calculations. Within the uncertainties associated with the analysis it is hard to claim any discrepancy.

---

[1] I.G. Bearden et al., Phys. Lett B **523**, 227(2001).
[2] I.G. Bearden et al., Phys. Rev. Lett. **88**, 202301(2002).
[3] H. Ito and S. J. Sanders, Brahms Analysis Note
[4] H. Ito, University of Kansas Ph.D. dissertation, unpublished (2002).